

https://doi.org/10.1070/QEL17585

Analysis of uncertainties of a cold-ytterbium atomic frequency standard using operational parameters of its optical lattice

A.V. Semenko, G.S. Belotelov, D.V. Sutyrin, S.N. Slyusarev,
V.I. Yudin, A.V. Taichenachev, V.D. Ovsiannikov, V.G. Pal'chikov

Abstract. **We have assessed the effect of optical lattice laser field parameters (polarisation, intensity, and wavelength) of a cold-ytterbium atomic frequency standard on the systematic uncertainty of precision clock transition frequency measurements. The spectrum and polarisation of the laser field of the lattice have been investigated in detail directly in the spatial region of interaction of cold ytterbium atoms with the laser field. The Stark shift of the clock transition in the vicinity of the magic wavelength of the laser has been estimated as a function of the experimentally measured laser field intensity in the dipole approximation. The estimates have been used to calculate the residual systematic uncertainty in the light shift of the optical lattice laser frequency.**

Keywords: *cold-ytterbium atomic frequency standard, portable frequency standard, magic intensity, magic polarisation, magic wavelength, light shift.*

1. Introduction

Frequency standards based on optical transitions (optical frequency standards, OFS's) have made an essential contribution to improving time and frequency measurement accuracy [1–3]. The best OFS's, based on atomic strontium transitions, offer a relative uncertainty under 10^{-18} [4, 5], but the residual systematic uncertainty (RSU) can be further reduced by optimising OFS parameters, such as the 'magic' wavelength [6], 'magic' intensity [7, 8], and 'magic' polarisation [9]. Such optimisation is of particular interest in the case of portable OFS's because the accommodation of an entire system in a small volume [10] imposes significant limitations on the size of the laser systems for use in OFS's. This circumstance makes it necessary to use diode laser systems, whose noise characteristics are inferior to those of solid-state systems.

A.V. Semenko, G.S. Belotelov, D.V. Sutyrin, S.N. Slyusarev
All-Russian Research Institute of Physical and Radio Engineering Measurements, 141570 Mendeleevo, Moscow region, Russia;
V.I. Yudin, A.V. Taichenachev Institute of Laser Physics, Siberian Branch, Russian Academy of Sciences, prosp. Akad. Lavrent'eva 15B, 630090 Novosibirsk, Russia; Novosibirsk State University, ul. Pirogova 2, 630090 Novosibirsk, Russia;
V.D. Ovsiannikov Voronezh State University, Universitetskaya pl. 1, 394018 Voronezh, Russia;
V.G. Pal'chikov All-Russian Research Institute of Physical and Radio Engineering Measurements, 141570 Mendeleevo, Moscow region, Russia; National Nuclear Research University MEPhI, Kashirskoe sh. 31, 115409 Moscow, Russia; e-mail: vitpal@mail.ru

Received 18 March 2021
Kvantovaya Elektronika **51** (6) 484–489 (2021)
Translated by O.M. Tsarev

The magic intensity for Sr, Yb, and Hg atoms has been the subject of a number of studies [7, 8, 11]. For Sr, researchers found the intensity range of an optical lattice laser (OLL) where the light shift of the clock frequency was minimised. Since no magic intensity has been found to date for Yb atoms, one topical issue is the ability to maintain the OLL frequency in a predetermined range where the light shift is as small as possible. Brown et al. [12] experimentally studied the effect of the optical lattice field on the frequency shift of an Yb optical standard in a wide range of OLL frequency detunings (–50 to 30 MHz) from the magic frequency. Unfortunately, they did not investigate the variation of the frequency shift in the vicinity of the magic wavelength (frequency detuning of hundreds of kilohertz).

Katori et al. [6] determined for the first time the magic wavelength for strontium atoms, at which the shifts of the upper and lower energy levels of the clock transitions coincide, allowing one to get rid of the first-order Stark shift. Typically used in laboratory frequency standards, Ti:sapphire lasers are unsuitable for portable systems because of their large size, which causes one to employ more compact diode lasers as OLLs. To raise their output power, use is made of optical amplifiers, in which amplified spontaneous emission (ASE) may cause a relative light shift of up to several parts in 10^{15} [13].

The concept of magic polarisation, which makes it possible to minimise the effect of second-order shifts, was proposed by Taichenachev et al. [9]. It is difficult to verify because, during experiments, the OLL output polarisation in a vacuum chamber is hard to monitor with high accuracy.

In this study, we have produced a pilot system for investigation of the OLL diode output polarisation, studied ASE spectra of the diode laser, and estimated the Stark shift of the clock transition near the magic wavelength in order to obtain numerical values of the light shift and its contribution to the RSU.

2. Calculation of the polarisability of ytterbium atom 'clock' levels in the optical lattice field

The key characteristics of an optical lattice are the OLL output intensity and wavelength. Knowledge of the intensity is crucial for determining the depth of the Stark potential that ensures reliable confinement of an atom in a limited region of space in a bound state with a preset vibrational quantum number. The choice of the magic wavelength is dictated by the necessity to equalise the Stark shifts of the clock levels in the lattice field, as a result of which the frequency of the clock transition is independent of the vibrational state of the atom trapped by the lattice. The major contribution to the depth of

the potential is made by optical lattice wavelength-dependent polarisabilities of working states. Because of this, the main condition in choosing the magic frequency of the lattice is that the dynamic polarisabilities of the clock levels be equal.

The shift of the levels involved in a clock transition in the field of a standing wave is due to the well-studied Stark effect in an ac field E and can be described in the most general form by the relation [14]

$$\nu = \nu^{(0)} - \frac{1}{4}\Delta\alpha(\boldsymbol{e},\omega)E^2 - \frac{1}{64}\Delta\gamma(\boldsymbol{e},\omega)E^4 - \ldots, \quad (1)$$

where $\nu^{(0)}$ is the frequency of the transition between the unperturbed atomic states and $\Delta\alpha(\boldsymbol{e},\omega)$ and $\Delta\gamma(\boldsymbol{e},\omega)$ are the differences in polarisability and hyperpolarisability between the excited and ground states involved in the clock transition. These differences depend on both the frequency ω and polarisation vector $\boldsymbol{e}$ of the OLL output. Polarisability can, in turn, be expanded in terms of multipole moments:

$$\alpha(\boldsymbol{e},\omega) = \alpha_{\mathrm{E1}}(\boldsymbol{e},\omega) + \alpha_{\mathrm{M1}}(\boldsymbol{e},\omega) + \alpha_{\mathrm{E2}}(\boldsymbol{e},\omega) + \ldots, \quad (2)$$

where we use standard notation for electric dipole (E1), magnetic dipole (M1), and electric quadrupole (E2) moments.

Qualitative estimates, first made by Katori et al. [6], show that, at typically used lattice laser intensities ($\sim$10 kW cm^{-2}), the Stark shift of the clock transition frequency as a result of hyperpolarisability of atomic states does not exceed a few hundredths of a hertz. At lattice laser frequencies approaching the magic frequency, the following smallness relation holds:

$$\alpha_{\mathrm{E2}}(\boldsymbol{e},\omega) \approx \alpha_{\mathrm{M1}}(\boldsymbol{e},\omega) \approx 10^{-7}\alpha_{\mathrm{E1}}(\boldsymbol{e},\omega).$$

Thus, to a first approximation the lattice laser-induced frequency shift depends only on the difference between the dipole polarisabilities of the excited and ground states of the clock transition.

At the same time, as shown by Katori et al. [11], taking into account higher order nonlinear optical effects (multipole character of light, anharmonicity of vibrational modes of atoms on lattice sites, hyperpolarisability of atomic states, and others) in interpreting precision OFS frequency measurement results (accuracy from 10^{-17} to 10^{-18}) makes it necessary to modify relation (1), and the lattice field-induced clock transition frequency shift with allowance for corrections quadratic in field intensity I can be represented in the form [11]

$$\Delta\nu_{\mathrm{cl}}^{\mathrm{latt}}(n_\nu,\delta,I) = c_{1/2}(n_\nu,\delta)I^{1/2} + c_1(n_\nu,\delta,\xi)I + c_{3/2}(n_\nu,\xi)I^{3/2} + c_2(\xi)I^2. \quad (3)$$

Here, n_ν is the vibrational quantum number; $\delta = \omega - \omega_{\mathrm{m}}^{\mathrm{E1}}$ is the difference between the OLL frequency and the magic frequency $\omega_{\mathrm{m}}^{\mathrm{E1}}$ for the electric dipole polarisabilities of the clock levels; and ξ is the degree of circular polarisation of the OLL.

Detuning the OLL frequency in the vicinity of magic wavelengths, we can minimise the field-dependent coefficients c in (3). The coefficients with fractional subscripts at the intensity I in (3) result from the square-root variation of the vibrational eigenfrequencies of an atom in the potential of the lattice [11]. In particular, the coefficient $c_{1/2}$ is determined by a combination of the polarisabilities (2) of the ground and excited states of the clock transition. The term linear in I is mainly determined by the difference between their electric dipole polarisabilities. In addition, a substantially smaller correction for hyperpolarisability to this term originates from the anharmonicity of vibrational modes of the atom. The coefficients c_1, $c_{3/2}$, and c_2 depend on the difference between the hyperpolarisabilities appearing in the definition of the eigenfrequencies and depths of the potential wells that confine atoms in the optical lattice.

Preliminary analysis of experimental data on the optical lattice field in subsequent sections of this paper shows that taking into account higher order nonlinear optical effects in frequency shift calculations leads to a clear improvement in accuracy in the case under consideration, which in turn allows only the first two terms in (1) to be retained in our calculations.

In this study, dynamic polarisabilities of the energy levels of the clock transition were calculated in the single-electron Fues model potential (FMP) approach [14], using empirical parameters evaluated from known atomic level energies [15, 16]. The most reliable numerical calculation results are ensured by the use of the FMP for monovalent atoms and ions having one outer (optical) electron. In the case of atoms having two or more optical electrons whose one-electron excitation spectrum partially overlaps with two-electron excitation spectra, the use of the FMP requires additional modification of empirical parameters. Such modification, i.e. the use of additional criteria for choosing FMP parameters, ensures good agreement between calculated magic wavelengths of alkaline-earth divalent atoms and the most accurate experimental data [11]. Yb atom polarisabilities obtained with a modified model potential are also similar to the most reliable theoretical and experimental values available in the literature [17]. Figure 1 presents the energy shift $\Delta E = -\alpha_{\mathrm{e(g)}}I$ calculated for the Yb clock levels by a modified FMP method.

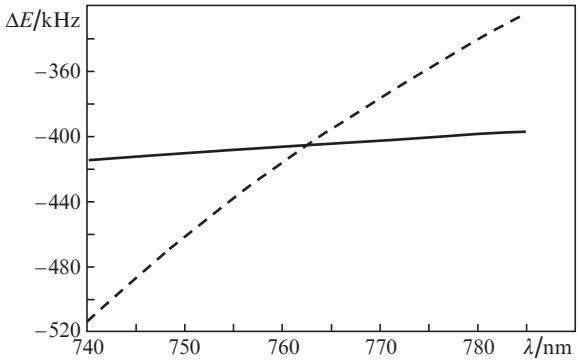

Figure 1. Energy shift $\Delta E = -\alpha_{\mathrm{e(g)}}I$ as a function of wavelength at a laser field intensity I = 10 kW cm^{-2} for Yb atoms in an excited state, $6s6p\,^3P_0$ (dashed line), and the ground state, $6s^2\,^1S_0$ (solid line), of the clock transition. The magic wavelength calculated in the model potential approach (762.6 nm) agrees well with experimental data (759.3537 nm) [17].

The effectiveness of modifying the FMP method was first demonstrated by Derevianko et al. [18]. Subsequently, this approach was successfully used in calculations of polarisabilities, hyperpolarisabilities, interactions of atoms with external fields, dynamic interactions, etc. (see e.g. Refs [14, 18, 19]). In this study, a modified FMP was used to calculate the polaris-

abilities of the clock levels of ytterbium atoms in the wavelength range 740–780 nm, where most of the diode laser ASE is located. These quantities were then used to evaluate the contribution to the uncertainty of an Yb atom frequency standard due to the spontaneous emission of the optical amplifier (emission of the diode laser). Details of numerical calculations of such a contribution are completely analogous to those of the uncertainty of a strontium atom frequency standard [19].

The main idea underlying FMP modification is as follows: First of all, we introduce noninteger orbital momenta of triplet S states, $l'_{^3S}$, which should nevertheless differ little from the real momenta of S states, $l'_{^3S} \approx l_S = 0$, and the effective momenta of singlet and triplet D states should satisfy the equality $l'_{^3D} \approx \tilde{l}_{^1D} \approx l_D = 2$. This choice leads to redefinition of the integer radial quantum number n_r, ensuring the original equality $l'_{^3S} + n_r + 1 = \tilde{n}_{nl}$ for the effective principal quantum number $\tilde{n}_{nl}$, which can be determined from the energy $E_{nl} = -Z^2/(2\tilde{n}_{nl}^2)$ of the $|nl\rangle$ atomic state.

This modification of the FMP method was used in this study in calculating the entire set of characteristics for Yb atoms. The magic wavelength calculation results presented in Fig. 1 agree well with the most reliable data in the literature [5, 11, 17], thus confirming the reliability of the modification.

3. Experimental

Figure 2 shows a schematic of a pilot system which can be used to study spectra and polarisation of laser light. The beam of a Moglabs diode laser emitting at a wavelength of 759.4 nm is launched into a polarisation-maintaining single-mode fibre. The beam emerging from the fibre passes through a half-wave and a quarter-wave plate for polarisation control. Lenses with a focal length $f = 250$ mm produce a beam waist in a pilot vacuum chamber, which contains a detection system with a polarimeter. At the laser beam waist, a laser beam profiler was located, which was used to determine the beam waist size: 40 × 40 μm. Polarisation was measured in the waist region and after the beam passed through both windows of the vacuum chamber. The spectrum was also measured in the waist region. The pilot chamber can be rotated around its axis to determine the polarisation after the beam passed through different points in the windows of the vacuum chamber. Inside the chamber, normal atmospheric pressure is maintained, but the windows are slightly curved because they are tightly secured to the chamber. In our experiment, we used CF40 vacuum windows fabricated using borosilicate glass (Kodial).

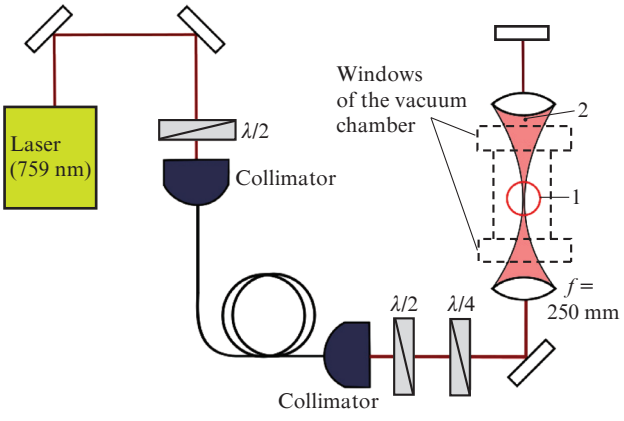

Figure 2. Experimental setup for measuring the laser output spectrum, beam profile, and beam polarisation. At point 1, the laser beam polarisation and profile at the focal waist are measured. At point 2, the polarisation and spectrum of the laser beam transmitted through the windows of the vacuum chamber are measured. In the pilot vacuum chamber, no vacuum is produced, but its windows are slightly curved (see Fig. 6).

4. Magic intensity

Katori et al. [7] examined how the frequency shift of a clock transition varied with the OLL frequency detuning from the magic frequency at various laser output intensities. Whereas in the case of strontium there is a narrow magic intensity range where the OLL frequency can be tuned to the magic frequency to within a few megahertz, in the case of ytterbium atoms there is essentially no magic intensity range. In this case, we can consider a magic detuning of the OLL frequency. At OLL output intensities below 30 kW cm^{-2}, the frequency shift is essentially a linear function of intensity. To obtain a clock transition frequency shift of $\sim 1 \times 10^{-18}$ at the magic detuning, the frequency should be stabilised to within 200 kHz at an intensity $I = 10$ kW cm^{-2} and to within 100 kHz at $I = 20$ kW cm^{-2} [7] (Fig. 3).

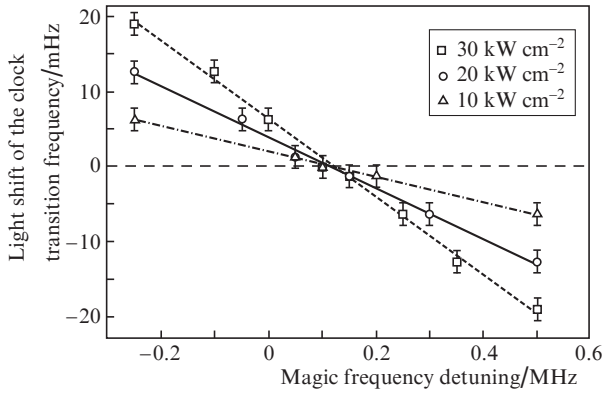

Figure 3. Light shift of the clock transition frequency vs. magic frequency detuning at different intensities I.

To make an OFS with a frequency uncertainty of 10^{-18}, the magic wavelength should be determined with an accuracy of ~100 kHz. State-of-the-art commercial laser systems without frequency stabilisation have an emission linewidth of the order of hundreds of kilohertz. Therefore, to ensure an RSU under 10^{-18}, the OLL frequency should be stabilised.

5. Magic wavelength and emission spectra of the diode laser

To produce an optical lattice, one should use a clear narrow spectrum of magic wavelength laser emission. Such a spectrum is offered by a Ti:sapphire solid-state laser [20], which is, however, poorly suited for portable systems because it has a large size and requires periodic alignment. Diode lasers have a compact design, consume less power, and have the required structural stability for transportation. A distinctive feature of the diode laser used in this study is the presence of an interference filter which forms a clean laser emission spectrum.

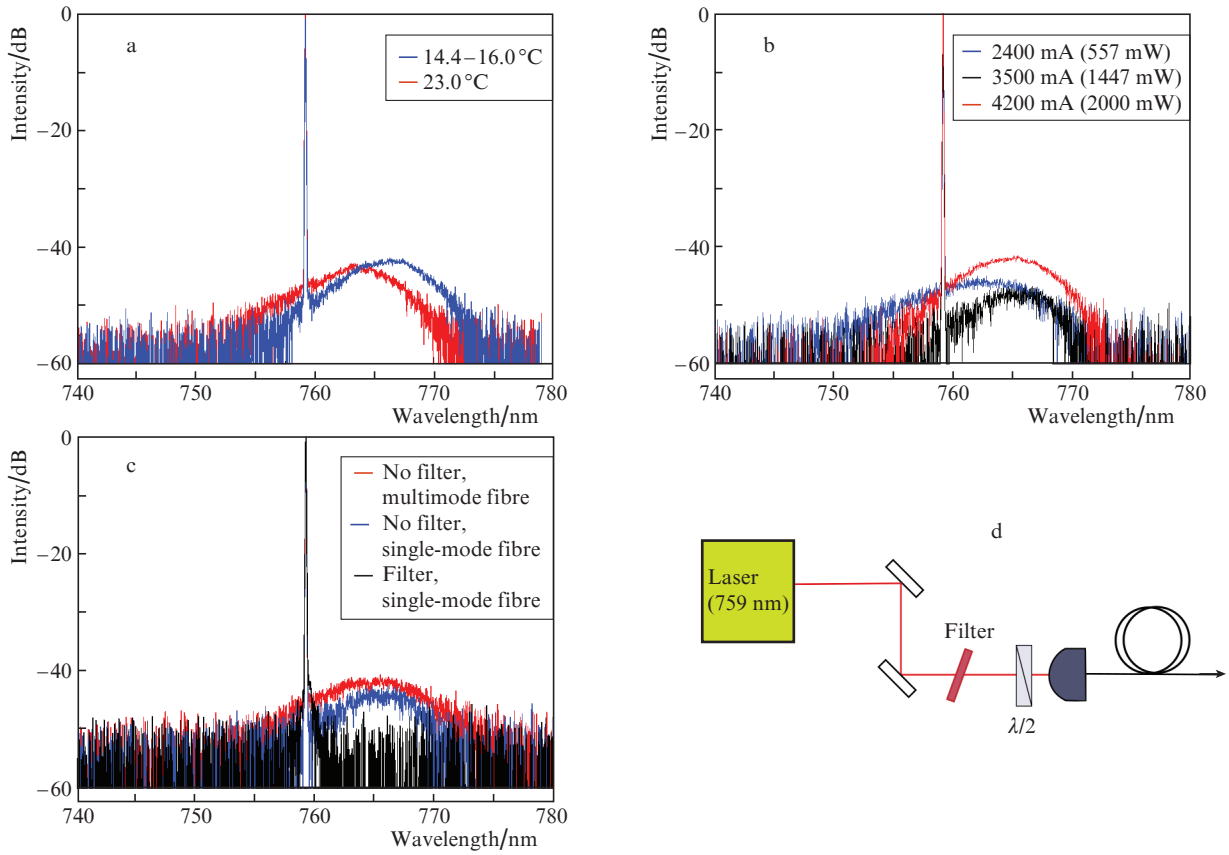

Figure 4. (Colour online) ASE spectra at different diode temperatures (a) and amplifier currents (b), emission spectra obtained at the outputs of multimode and single-mode fibres and at the output of single-mode fibre with the use of an interference filter (c), and schematic of the experimental setup containing an interference filter (d).

However, to obtain an optical power sufficient for confining atoms in an optical lattice, an optical amplifier is needed. It produces emission spectrum components whose polarisation is difficult to control because the shape of the ASE envelope depends on temperature and amplifier current [21].

Figure 4 shows ASE spectra at different diode temperatures and amplifier currents. The rated working temperature of the Moglabs diode is 23 °C, but it is seen from Fig. 4a that the emission spectrum is cleaner at lower temperatures. Moreover, the diode temperature influences the laser output power as well. The amplifier current also has a strong effect on the emission spectrum of the laser. The cleanest spectrum with the optimal output power was obtained at an amplifier current of 3500 mA. The output power was 1.5 W.

At an insufficiently clean laser emission spectrum at the output of the optical amplifier, the ASE pedestal (background) can be reduced using an optical filter (Fig. 4d). Figure 4c shows emission spectra obtained at the outputs of multimode and single-mode fibres and at the output of single-mode fibre with the use of an interference filter in the experimental setup.

It is seen from Fig. 4c that the filter allows ASE to be almost completely eliminated, but this is accompanied by rather large power losses. Since a large depth of the optical lattice potential is needed for atom confinement ($U > 350E_r = 700$ kHz, where $E_r = 2$ kHz is the photon recoil energy at the magic frequency [11]), it is necessary to estimate the corresponding light intensity $I = 2P/(\pi w_0^2)$, where P is the output power and w_0 is the laser beam waist radius in the region of optical lattice formation. The depth of the optical lattice, $U = \alpha_{g(e)}(\omega_m)I$, is determined by the product of the intensity and the dynamic polarisability of the clock levels [ground (g) or excited-state (e) level]: $\alpha_g(\omega_m) = \alpha_e(\omega_m) = 40.5$ kHz kW^{-1} cm^2 [7, 11].

The thermal energy of ytterbium atoms cooled to a temperature $T \approx 20$ μK is $E_T = \frac{3}{2}k_B T = 626$ kHz $\approx 313E_r$. Using lenses with a focal length $f = 250$ mm, we were able to obtain an OLL beam waist radius at half maximum $w_0 \approx 40$ μm. At an optical power of 1 W, this corresponds to an optical lattice depth $U = 1612$ kHz $\approx 806E_r$. At $w_0 = 50$ μm, we obtain $U = 1032$ kHz $\approx 516E_r$; at $w_0 = 100$ μm, we have $U = 258$ kHz $\approx 130E_r$. Therefore, the available laser power may be quite sufficient for atoms cooled to 20 μK to be confined in an optical lattice.

We estimated the OLL frequency shift after the optical amplifier and after the optical fibre. As a result of unfiltered ASE, the maximum shift is -6.09 (± 3.70) Hz, or -1.34×10^{-14} ($\pm 0.70 \times 10^{-14}$) in relative units. The rather large uncertainty in the clock transition frequency is due to the asymmetry of the spectrum. In the case of filtered light, the shift is about $-0.01(\pm 0.33)$ Hz, or -1.84×10^{-17} ($\pm 0.63 \times 10^{-17}$). The analogous uncertainty in the optical lattice laser frequency in strontium systems [19] is 2.60×10^{-16}.

6. Magic polarisation

After elimination of the effect of ASE, one of the most important shifts is the shift of second order in lattice field intensity.

The third term in (1) represents corrections to the clock transition frequency due to the hyperpolarisabilities of the atomic states of this transition, which depend on the frequency and polarisation of the optical lattice field. The existence of a magic polarisation at which the effect of the shifts of second order in field intensity can be minimised is a hypothesis, first formulated by Taichenachev et al. [9]. The theoretical estimates made by them indicate that the optical lattice field polarisation should have the shape of an ellipse with an ellipticity coefficient of ~0.7. To experimentally confirm this hypothesis, it is necessary to investigate a wide variety of effects and experimental conditions, in particular to study variations of the polarisation as the beam passes through various optical components.

One component influencing the laser beam polarisation is optical fibre. We investigated temporal polarisation stability at the output of a temperature-stabilised polarisation-maintaining single-mode fibre. Over the observation time (8 h), the polarisation angle changed by no more than 2°, and the ellipticity angle, by no more than 1° (Fig. 5). Thus, if fibre is temperature-stabilised, polarisation varies in it only slightly.

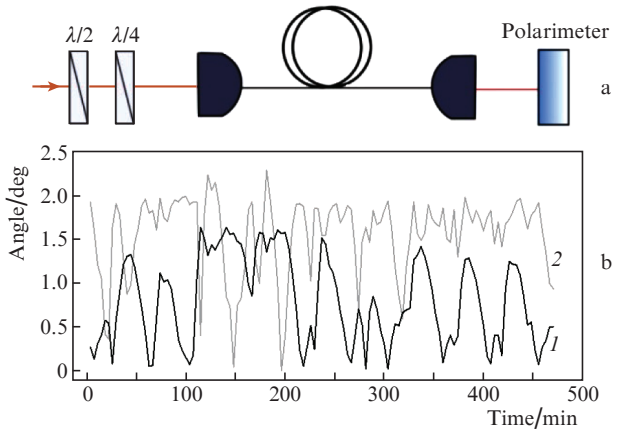

Figure 5. Variation of polarisation in a polarisation-maintaining single-mode fibre: (a) schematic of the pilot configuration and (b) time dependences of the (*1*) ellipticity and (*2*) azimuth angles.

Another optical component capable of unpredictably changing beam polarisation is the windows of the vacuum chamber. Here, polarisation is distorted as a result of the birefringence induced by the stress in the tightly secured windows of the chamber [22]. At present, we model this effect in relation to the coupling bolt torque for fastening the vacuum windows. Note that a torque of 5 N m leads to bending of the window, with the maximum displacement in its centre reaching 0.35 nm (Fig. 6).

It was shown experimentally that the beam polarisation was indeed distorted as the beam passed through the windows of the vacuum chamber. In our experiment, the beam passed through the two windows of the vacuum chamber at normal atmospheric pressure and was detected at the exit by a polarimeter. As a result, the ellipticity angle increased by ~3.5° for the linear and elliptical beam polarisations.

Moreover, the change in polarisation varied from point to point because of the nonuniform stress distribution over the windows of the vacuum chamber [23]. We evaluated the polarisation of the laser beam passing through one of the windows of the vacuum chamber ~5 mm from its centre while the

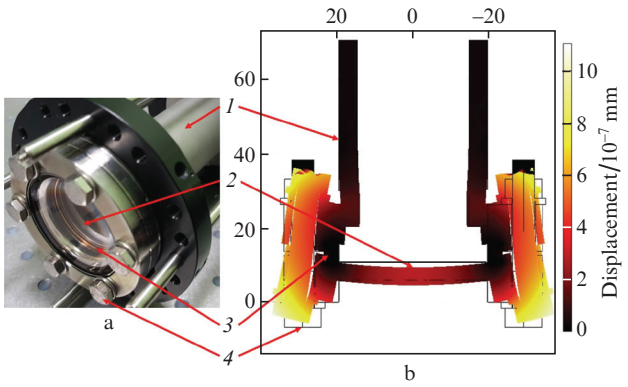

Figure 6. (Colour online) (a) Photograph of a part of the vacuum chamber and (b) simulation of the bending of the chamber window at a coupling bolt torque of 5 N m, which is equivalent to a pressure of 4000 N m^{-2} on the gasket. The displacement in the centre of the window is 0.35 nm. The vertical and horizontal axes represent the dimensions of the pilot chamber in millimetres: (*1*) part of the vacuum chamber; (*2*) vacuum window; (*3*) copper gasket; (*4*) bolts fastening the vacuum window.

chamber was rotated around its axis. The results are presented in Fig. 7 in polar coordinates for linear and elliptical polarisations. Since the ellipticity angle of elliptically polarised light changes by no more than 1.5°, and the polarisation angle, by no more than 0.2°, this effect has no significant influence on the magic polarisation.

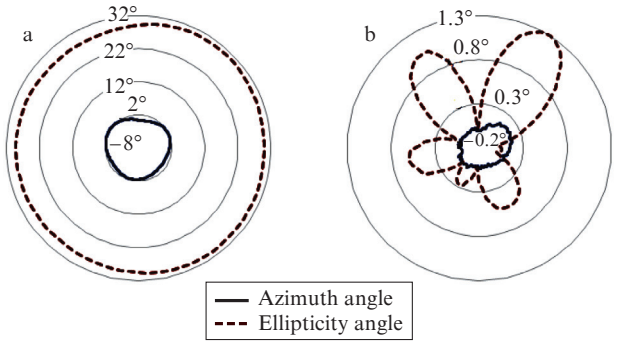

Figure 7. Variation of beam polarisation as the beam passes through the windows of the vacuum chamber in the case of (a) linear and (b) elliptical polarisations.

Investigation with the use of the pilot vacuum chamber and subsequent simulation results will provide necessary information about the accuracy with which one will be able to monitor the polarisation angle in the vacuum chamber in cold atom experiments.

7. Conclusions

The Stark shift of the clock transition frequency in the vicinity of the magic wavelength of a laser has been estimated as a function of the experimentally measured laser field intensity in the dipole approximation. The estimates have been used to calculate the RSU in the light shift of the optical lattice laser frequency. The optical spectrum and polarisation of the laser field of the lattice have been studied experimentally directly in the spatial region of interaction of cold ytterbium atoms with

the laser field. In addition, we have experimentally studied the effect of all optical components, including the windows of the vacuum chamber, on laser beam polarisation and demonstrated that the polarisation angle varies only slightly and is stable over time. According to our estimates, the noise introduced into the spectrum of the optical lattice field by the optical amplifier can lead to a frequency shift at a level of a few parts in 10^{16}. The optical lattice laser field parameters estimated in this study will be used in designing a portable cold-ytterbium atomic OFS.

Acknowledgements. This work was supported by the RF Ministry of Science and Higher Education (state research task, Project Nos FZGU-2020-0035 and FSUS-2020-0036), the Russian Foundation for Basic Research (Grant Nos 20-02-00505 and 20-52-12024), the BASIS Foundation for the Development of Theoretical Physics and Mathematics, and the Russian Science Foundation (Grant Nos 20-12-00081 and 19-72-30014).

References

1. Marti G.E., Hutson R.B., Goban A., Campbell S.L., Poli N., Ye J. *Phys. Rev. Lett*., **120**, 103201 (2018).
2. Bothwel T., Kedar D., Oelker E., Robinson J.M., Bromley S.L., Tew W.L., Ye J., Kennedy C.J. *Metrologia*, **56** (6), 065004 (2019).
3. Beloy K., Bodin M.I., Bothwell T., et al. *Nature*, **591** (7851), 564 (2021).
4. Bloom B.J., Nicholson T.L., Williams J.R., Campbell S.L., Bishof M., Zhang X., Zhang W., Bromley S.L., Ye J. *Nature*, **506**, 71 (2014).
5. Ushijima I., Takamoto M., Das M., Ohkubo T., Katori H. *Nat. Photonics*, **9**, 185 (2015).
6. Katori H., Takamoto M., Pal'chikov V.G., Ovsiannikov V.D. *Phys. Rev. Lett.*, **91**, 173005 (2003).
7. Katori H., Ovsiannikov V.D., Marmo S.I., Palchikov V.G. *Phys. Rev. A*, **91** (5), 052503 (2015).
8. Ushijima I., Takamoto M., Katori H. *Phys. Rev. Lett*., **121**, 263202 (2018).
9. Taichenachev A.V., Yudin V.I., Ovsiannikov V.D., Pal'chikov V.G. *Phys. Rev. Lett*., **97**, 173601 (2006).
10. Koller S.B., Grotti J., Vogt St., Al-Masoudi A., Dörscher S., Häfner S., Sterr U., Lisdat Ch. *Phys. Rev. Lett*., **118**, 073601 (2017).
11. Katori H., Ovsiannikov V.D., Marmo S.I., Palchikov V.G. *Phys. Rev. A*, **93**, 043420 (2016).
12. Brown R.C. et al. *Phys. Rev. Lett*., **119**, 253001 (2017).
13. Fasano R.J. et al. arXiv preprint arXiv:2103.12052 (2021).
14. Manakov N.L., Ovsiannikov V.D., Rapoport L.P. *Phys. Rep*., **141**, 319 (1986).
15. Ralchenko Yu., Kramida A., Reader J. http://physics.nist.gov/asd (2020).
16. Kazakov V.V., Kazakov V.G., Kovalev V.S., Meshkov O.L., Yatsenko A.S. *Phys. Scr*., **92** (10), 105002 (2017).
17. Barber Z.W., Stalnaker J.E., Lemke N.D., et al. *Phys. Rev. Lett*., **100**, 103002 (2008).
18. Derevianko A., Johnson W.R., Ovsyannikov V.D., Pal'chikov V.G., Plante D.R., von Oppen G. *J. Exp. Theor. Phys*., **88**, 272 (1999) [*Zh. Eksp. Teor. Fiz*., **115**, 494 (1999)].
19. Belotelov G.S., Ovsiannikov V.D., Sutyrin D.V., Gribov A.Yu., Berdasov O.I., Pal'chikov V.G., Slyusarev S.N., Blinov I.Yu. *Laser Phys*., **30**, 045501 (2020).
20. Lodewyck J., Bilicki S., Bookjans E., Robyr J., Shi Ch., Vallet G., Targat R.L., Nicolodi D., Le Coq Y., Guena J., Abgrall M., Rosenbusch P., Bize S. *Metrologia*, **53**, 1123 (2016).
21. Bogatov A.P., Drakin A.E., D'yachkov N.V., Gushchik T.I. *Quantum Electron*., **46**, 693 (2016) [*Kvantovaya Elektron*., **46**, 693 (2016)].
22. Steffen A., Alt W., Genske M., Meschede D., Carsten R., Alberti A. *Rev. Sci. Instrum*., **84**, 126103 (2013).
23. Solmeyer N., Zhu K., Weiss D.S. *Rev. Sci. Instrum*., **82**, 066105 (2011).